Downstream Separation of Formic Acid with Anion-exchange Resin from Electrocatalytic Carbon Dioxide (CO_2) Conversion: Adsorption, Kinetics, and Equilibrium Modeling

*Md A. Hoque[1,2], Keemia Abad[1,2,3], Pom Kharel[1,2], Ayo Omosebi[1,2], and Jesse Thompson[1,2,3]**

[1]Institute for Decarbonization and Energy Advancement, University of Kentucky, 1 Quality Street, Lexington, Kentucky 40507, United States

[2]Center for Applied Energy Research, University of Kentucky, 2540 Research Park Drive, Lexington, Kentucky 40511, United States

[3]Department of Chemistry, University of Kentucky, 161 Jacobs Science Building, Lexington, Kentucky 40506, United States

*Email: jesse.thomposn@uky.edu

Abstract

Electrocatalytic carbon dioxide reduction reaction (CO_2RR) to produce liquid formic acid (FA) is one potential route to minimize the CO_2 concentration in the atmosphere by utilizing CO_2 as a feedstock. However, one of the main disadvantages in this route is the high energy demand required for purification through conventional distillation. This method of purification has been shown to result in a high carbon footprint in life-cycle analysis (LCA). Therefore, finding an alternative purification technique that can integrate with an electrochemical CO_2RR process with the potential to lower the carbon footprint would be of great interest. Under the experimental conditions of CO_2RR, FA remains in its basic form as the formate anion in the catholyte. Anion Exchange resins with their basic properties can separate the formate anion from the catholyte mixture as an alternative to energy intensive distillation. In this work, three anion exchange resins with increasing basicity order: Amberlite IRA-96 < Amberlite IRA-910 < Ambersep 900 are tested to separate FA in the presence of aqueous solution of potassium bicarbonate catholyte with varying levels of resin and FA. Kinetics and equilibrium studies data for the FA adsorption are interpreted using several kinetics and isotherm models. The kinetics data fits well with a pseudo first order model at high initial FA concentrations and a pseudo second order model at low initial FA concentrations. The experimental data can be best explained with the Freundlich isotherm model. The fitted results show that strongly basic Ambersep 900 is more effective at separating FA, with a maximum adsorption capacity of 336.7 mg/g compared to Amberlite IRA-96 (275.2 mg/g) and Amberlite IRA-910 (209.2 mg/g) in neutral water. However, weakly basic Amberlite IRA-96 (110.8 mg/g) can separate FA more efficiently from the potassium bicarbonate catholyte, than Amberlite IRA-910 (99.9 mg/g) and Ambersep 900 (40.0 mg/g). Competitive adsorption occurs in the presence of potassium bicarbonate catholyte, but the formic acid adsorption capacity is still sufficient for adequate separation.

1. INTRODUCTION

Carbon capture and utilization (CCU) technology has achieved great interest in recent years to mitigate CO_2 emissions in the atmosphere by converting it into valuable chemicals and fuels in comparison to carbon capture and sequestration (CCS).[1-5] Among several utilization technologies, electrocatalytic CO_2 reduction reaction (CO_2RR) into fuels and value-added chemicals is a promising approach for utilizing the CO_2 as a feedstock in terms of economic feasibility and environmental sustainability.[6-10] Formic acid (FA) is one of the important C1 chemicals that can be produced from electrocatalytic CO_2R.[6-8, 11, 12] It has a large industrial value because of its widespread use as a feedstock in pharmaceuticals, foods, leathers, tannings, and textile industries.[13-15] In addition, it has a promising potential larger commercial market due to its storage capacity for hydrogen (through its reversible decomposition back to CO_2 and H_2), with the possibility of regenerating FA and providing power from a formic acid fuel cell.[13-17] A wide range of molecular complex (Cu, Co, Mn, etc.) and metal based (Sn, In, Rh, Ni, Cu, etc.) electrocatalysts are used as cathode for electrochemical CO_2R reaction.[18-20 21-24] Novel electrochemical reactor designs have also been developed to improve the CO_2R reaction both in terms of Faradaic efficiency and formic acid production. Yang, et al. studied the direct conversion of $CO_2(g)$ into formic acid using a special design of three compartment cell electrolyzer and Sustainion TM membrane in separate studies that produced formic acid without the need for an additional protonation step.[25, 26] Kaczur et al. purified produced formic acid in a CO_2RR by concentrating it from the formic acid-water system using pervaporation methods.[27] Electrocatalytic CO_2R reactions can be studied in either in H-type or flow-type cells and often use potassium bicarbonate as the catholyte with a CO_2 gas feed.[12, 28-30 11, 31-33] The reaction produces liquid FA (along with some other gaseous products) which stays in the mixture along with the electrolyte solution. [8, 10, 30, 33] However, producing high-purity commercial grade FA for industrial purposes requires separating liquid FA from the catholyte mixture.

Solvent extraction, distillation, membrane filtration, electrodialysis, crystallization, ion exchange and adsorption, etc., have been used to separate FA from aqueous solution in wastewater streams of pharmaceuticals, agriculture, foods, etc..[34-38] These techniques have some limitations for their use in industrial processes because of noteworthy effects on the environment or economic viability.[13, 39, 40] Distillation is a commonly used techniques for FA purification in several production processes including (i) reaction of methanol and CO to produce liquid FA at elevated temperature and pressure, (ii) homogenous catalytic production of FA from CO_2 and H_2, and (iii) electrochemical CO_2RR to FA.[41 42, 43 44]

The Life Cycle Analysis (LCA) on FA production using distillation as the purification technique shows large carbon footprint (CF).[45, 46] This high CF is mainly coming from the high steam demand using fossil fuels sources. The electricity consumption for electrochemical CO_2RR by per unit mass of FA ranges from 3.07-11.93 kWh.kg^{-1} for 30-1.68% FA outlet concentration, and the corresponding consumption of steam for purification per unit mass of FA was reported from a low of 14.90 MJ up to 401.00 MJ. The proportionally high steam consumption for purifying FA with distillation creates a great challenge towards utilizing CO_2 through electrochemical CO_2RR while targeting carbon neutrality. Therefore, a less energy intensive and sustainable purification method is required to minimize the CF for FA production. Ion exchange with adsorption has been shown as a viable advanced process for FA separation from dilute aqueous solution.[47] This method has advantages due to its high selectivity, low cost, ease of operation and recovery, availability to integrate with other systems, and environmentally benign nature.[48-50]

There are several published reports on the separation of FA using anion exchange resins (AERs) from aqueous solutions. In 1992, sorption equilibrium and batch dynamics for FA on AERs correlating effective ionic pore diffusion with experimental data were investigated.[14] Liu et al. in 2019 studied the D301, D315, and D1107 polymeric resins adsorbents to investigate the effects of levulinic acid on the adsorption of FA.[51] A series of parameters variation for example, pH, adsorbent dose, temperature and initial FA concentration, has been employed and evaluated on D-

1107 resin for FA separation.[47] The adsorption capacity of Amberlite IRA-67 has been tested for the resin loading of 23-115 mg.mL^{-1} along with the kinetics, thermodynamics and equilibrium.[39] Similar studies have been done by Hani et al. for Amberlite IRA-96 and Lewatit MP-64 in 2019.[13] Triegerman et al. in 2019 studied the adsorption of pure formate onto a strongly basic anion exchange resin (Dowes-Cl) along with the recovery of adsorbed formate into formic acid and regeneration of spent resin for the application of hydrogenation catalytic reaction mixture. But the sorption behavior of formate with AER will be significantly affected by the presence of other components of the mixture in cathode chamber. Therefore, it is important to study the separation of formate with best available AER by modeling the separation process in a real reaction mixture.[52] However, there is little information on the most effective resin with optimized conditions for FA separation from CO_2RR solution.

In CO_2RR with aqueous $KHCO_3$ electrolyte in cathode chamber, produced formic acid in reaction mixture stays as its basic form, formate anion.[6, 9, 13, 30, 53] During the separation of FA using AERs, the presence of $KHCO_3$ in aqueous solution may alter the process parameters and conditions due to competitive adsorption of bicarbonate on resin as found in similar studies for polymeric adsorbents.[51] Formic acid is a weakly acidic monocarboxylic acid with a pK_a of 3.75.[53] In an aqueous solution of pure formic acid and/or in the mixture of potassium bicarbonate solution, it can remain as undissociated formic acid and/or dissociated formate anion form based on the pH of the solution.[13, 53] Therefore, the adsorption mode on the resin surface will vary accordingly based on the basicity of the adsorption sites on the resin surface.[54] The formate anion may be efficiently separated from the catholyte mixture by using anion exchange resins of different basicity through adsorption and ion exchange mechanism.[47, 54] Therefore, studying and testing AERs to separate FA from electrocatalytic CO_2RR in the presence of $KHCO_3$ is important to report for the development of this technology. However, no study has been found in the literature employing AERs of different basicity to separate FA from $KHCO_3$ aqueous solution.

In this work, three anion exchange resins of different basicity from three available categories are chosen to determine their adsorption capacity for formic acid separation from neutral water and in presence of potassium bicarbonate. A strongly basic type-I resins, Ambersep 900 hydroxide form, strongly basic type-II resins (which are relatively weaker than type-I resin), Amberlite IRA-910, and a weakly basic resin, Amberlite IRA-96 free from are used to study the kinetics, equilibrium, and isotherm modeling of FA adsorption from aqueous solution. The adsorption capacity for the formic acid separation from potassium bicarbonate aqueous solutions are compared with the basicity of three AERs.

2. MATERIALS AND METHODS

2.1. Materials. Three anion exchange resins (AERs), including Amberlite IRA-96 free base form, Ambersep 900 hydroxide form, and Amberlite IRA-910 chloride form were purchased from Sigma Aldrich and used without any treatment as received. The characteristic properties and suggested operating conditions in the supplier-provided information for three resins are listed in Table S1. The formic acid (FA) of Optima LC-MS grade and potassium bicarbonate ($KHCO_3$) of 99.7% were purchased from Fisher Chemical and Sigma-Aldrich, respectively. Ultra-pure water (18.2 MΩ) was used to prepare all the samples.

2.2. Kinetics experiment. The kinetics for the adsorption of FA on resin from 10.0 mL of aqueous solution was conducted in a 50 mL centrifuge tube. The resin dose level of 20 mg/mL and the FA initial concentration, $[FA]_0$ of 0.05 M and 0.50 M, were used for the kinetics studies. Each FA solution was contacted with each of three AERs at the predetermined dose levels. In a typical kinetics experiment, the mixture of resin and FA was shaken for 2 hours at 22 °C with a rate of 400 rpm in a digital vortex mixer (Fisher Scientific) to maximize contact. An aliquot of 200.0 μL was withdrawn at 20 min intervals with the help of a syringe and needle, passed through a filter of 0.2 μm pore size to avoid any solid particles, and stored in plastic vials for the analysis of FA concentration using ion chromatography.

2.3. Adsorption from aqueous solution. Six different standard FA solutions with initial concentrations of 0.05 M, 0.10 M, 0.50 M, 1.00 M, 1.50 M, and 2.00 M were prepared in 10.0 mL of ultra-pure water (18.2 MΩ). Each FA solution was contacted with each of three AERs at the predetermined dose levels of 10, 20, 30, 40, 50, and 60 mg/mL in a 50 mL centrifuge tube. The mixture was shaken for 2 h at 22 °C temperature at a rate of 400 rpm for good contact to reach the adsorption-desorption equilibrium. The mixture rested for 5 min to separate the solid-liquid phases.

2.4. Adsorption from potassium bicarbonate electrolyte. Effects of potassium bicarbonate ($KHCO_3$) for FA adsorption on the resins were performed in a similar procedure as described earlier. Prior to the addition of resin, each of the FA solutions were mixed with $KHCO_3$ solution. The potassium bicarbonate initial concentration, $[KHCO_3]_0$ of 0.50 M with varying FA initial concentration was used with two different resin dose levels: 10 and 60 mg/mL. To understand the effects of variable $[KHCO_3]_0$, an experiment with 0.20 M of 10.0 mL aqueous solution of initial potassium bicarbonate was performed with 0.6 g of resin with varying FA initial concentrations (0.05 M–2.00 M). The pH of potassium bicarbonate solution, humid CO_2 bubbled $KHCO_3$ solution, and mixture of formic acid of varying initial concentration with CO_2 bubbled $KHCO_3$ solution was recorded using a pH meter to model the CO_2RR cathode chamber.

2.5. Ion chromatography analysis. The concentration of FA in the liquid phase was analyzed and quantified using calibration curve of standard formate anion using Ion chromatograph (Dionex ICS-6000, Thermo-scientific). The anion system consisted of an ADRS-600 2 mm suppressor, EGC 500 KOH (potassium hydroxide) eluent generator, IonPac AS15 analytical column and an AG15 guard column operated at 30 °C. The eluent gradient used an initial KOH concentration of 15.0 mM and increased to 60.0 mM at 12 min and held for 4 min with an injection volume of 10.0 μL sample. The samples were detected on the conductivity detector maintained at 30 °C. Certified standards of 1000 ppm formate (99.4000%, Inorganic Ventures) with a density of 1.000 g/mL were used for the preparation of calibration curve. The standards and samples were prepared with 18.2 MΩ water and injected for triplicate measurements. Peak identification and integration were performed using Dionex Chromeleon 7 Chromatography data system software version 7.2.8.

3. RESULTS AND DISCUSSION

3.1. Effects of contact time and initial formic acid concentration on adsorption. The adsorption quantity (q_t) at time, t, defined as the adsorbed amount of formic acid (FA) per unit mass of resin, rate of adsorption, and adsorption efficiency (%) of the resin are calculated using equation 1-3.[13, 47]

$$\text{Adsorption Quanity, } q_t = \frac{C_0 - C_t}{m} \times V \times M \ldots\ldots\ldots\ldots\ldots\ldots\ldots\ldots\ldots\ldots 1$$

$$\text{Rate of Adsorption (\%)} = \frac{\Delta q_t}{\Delta t} \ldots\ldots\ldots\ldots\ldots\ldots\ldots\ldots\ldots\ldots 2$$

$$\text{Adsorption Efficiecny (\%)} = \frac{C_0 - C_e}{C_0} \times 100 \ldots\ldots\ldots\ldots\ldots\ldots 3$$

where, C_0, C_t, and C_e are the FA concentration at time $t = 0$, t, and equilibrium, respectively, V is the volume of solution, M is the molar mass of FA, m is the mass of resin, and Δq_t is the change in adsorption quantity in a time interval of Δt. The adsorption capacity, (q_e) at equilibrium is calculated using C_e instead of C_t in equation 1.

The FA adsorption quantity, adsorption efficiency, and equilibrium contact time for the adsorption-desorption process from the Ambersep 900, Amberlite IRA-96, and Amberlite IRA-910 with $[FA]_0$ (FA initial concentration) of 0.05 M and 0.50 M for 120 min at room temperature is shown in Figure 1. The initial rate of adsorption (i.e., change in adsorption quantity in first 40 min) for strong base Ambersep 900 with low 0.05 M and high 0.50 M $[FA]_0$ is similar with 1.9 and 1.8 mg_{FA}/g_R/min, respectively. Unlike Ambersep 900, the initial rate of adsorption increases from 2.0 to 3.0 mg_{FA}/g_R/min for Amberlite IRA-96, and 0.24 to 1.19 mg_{FA}/g_R/min for Amberlite IRA-910 with the increase in initial FA concentration from 0.05 M to 0.50 M. However, with increasing contact time between resin and FA, the adsorption quantity reached equilibrium more quickly for low $[FA]_o$ but takes more time for the high $[FA]_0$ case for all three resins. At a fixed resin loading, the low initial absorption rate with low FA concentration is due to the availability of fewer FA molecules for the available resins sites, and vice versa with a high FA concentration. The adsorption rates are higher at the beginning of the contact time, then become lower, and finally reaches a plateau indicating adsorption-desorption equilibrium has been reached for all three resins irrespective of FA concentration and resins. This can be rationalized as all the surface sites of resins are initially available for the adsorption of FA with a high initial adsorption rate. With increase in contact time, the remaining free surface sites become more difficult for adsorption because of repulsion between adsorbent and adsorbates surfaces.[39]

The ion exchange adsorption efficiencies dropped with increasing initial concentration of FA at a fixed resin dose, with the low $[FA]_0$ adsorption efficiency being higher compared to high $[FA]_0$ except for the Amberlite IRA-910, which had an almost similar adsorption efficiency at both formic acid concentrations. The low adsorption efficiency with high $[FA]_0 = 0.50$ M for Ambersep 900 and Amberlite IRA-96 resin compared with $[FA]_0 = 0.05$ M can be related to the available surface sites of the resins. However, the almost similar adsorption efficiency for Amberlite IRA-910 with the low $[FA]_0$ and high $[FA]_0$ may be due to its greater adsorption capacity than the range of concentration studied. It is observed that with increases in contact time, both adsorption quantity and adsorption efficiency increase reaching an adsorption-desorption equilibrium plateau at 2 hours. All other adsorption experiments are performed for a contact time of 2 hours.

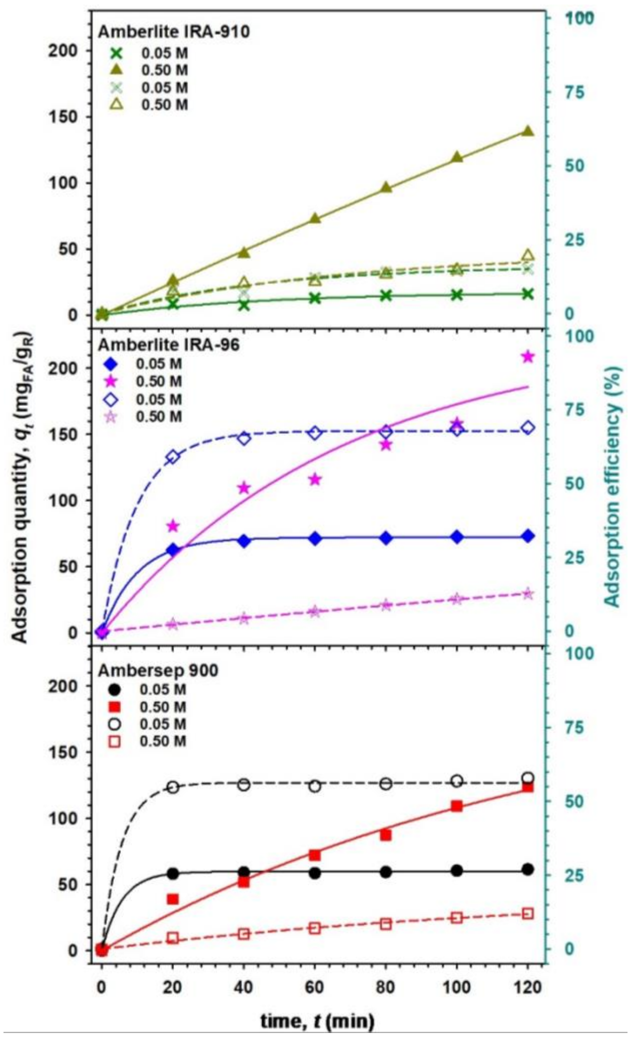

Figure 1. Effect of contact time on formic acid (FA) adsorption quantity, qt (black left axis) and adsorption efficiency (cyan right axis) of Ambersep 900 (bottom), Amberlite IRA-96 (middle), and Amberlite IRA-910 (top) with resin loading of 20 mg/mL in 10.0 mL aqueous solution with

FA initial concentration, $[FA]_0$ of 0.05 M and 0.50 M. Ambersep 900; $[FA]_0$ = 0.05 M (black circle) and 0.50 M (red square), Amberlite IRA-96; $[FA]_0$ = 0.05 M (blue diamond) and 0.50 M (pink star), Amberlite IRA-910; $[FA]_0$ = 0.05 M (green cross) and 0.50 M (yellow triangle), solid shape and solid line (adsorption quantity), empty shape and dashed line (adsorption efficiency), and mg_{FA}/g_R (milligrams of formic acid per gram of resin).

3.2. Kinetics modeling. Kinetic models such as Elovich, pseudo-first order (PFO), and pseudo-second order (PSO) can be used to analyze the adsorption data for each of the resins. The rate equation for these models is given by equation 3-5.[13, 47, 55]

Elovich; $\frac{dq_t}{dt} = \alpha.\exp(\beta.q_t)$ ……………………………………………………3

Pseudo first order; $\frac{dq_t}{dt} = k_1.(q_e - q_t)$ ……………………………………………………4

Pseudo second order; $\frac{dq_t}{dt} = k_2.(q_e - q_t)^2$ ……………………………………………………5

where q_t and q_e are the adsorbed FA in milligrams per gram of resin at time t, and equilibrium, respectively, t is the contact time of resin and FA, and β is the Elovich desorption constant. Elovich adsorption rate constant, PFO rate constant, and PSO rate constant are denoted by α, k_1, and k_2, respectively. To represent the best fit of the models to the experimental data, a linear form (equation 6-8) of the above three equations is used for plotting.[13, 50, 55]

Elovich; $q_t = \frac{1}{\beta}\ln(\alpha\beta) + \frac{1}{\beta}\ln t$ ……………………………………………………6

Pseudo first order; $\ln(q_e - q_t) = \ln q_e - k_1 t$ ……………………………………………………7

Pseudo second order; $\frac{1}{q_t} = \frac{1}{k_2 q_e^2} + \frac{t}{q_2}$ ……………………………………………………8

The appropriate linear fitting using the adsorption quantity data from Figure 1 provides the kinetic model constants which are listed in Table 1. The determination of coefficient (R^2) obtained from the linear fitting can best describe the experimental data. The best fit with highest R^2 values of

0.999 for Ambersep 900, 0.999 Amberlite IRA-96, and 0.996 for Amberlite IRA-910 with PSO kinetics modeling for $[FA]_0 = 0.05$ M. Upon increasing to $[FA]_0 = 0.50$ M, the experimental date follows the PFO kinetics with R^2 values of 0.923, 0.970, and 0.928 for Ambersep 900, Amberlite IRA-96, and Amberlite IRA-910, respectively. The fitted adsorption capacity at equilibrium, q_e with $[FA]_0 = 0.05$ M for the PSO modeling and $[FA]_0 = 0.50$ M for the PFO modeling also well match with the experimental data displayed in Figure 1. The corresponding R^2 values with $[FA]_0$ = 0.05 M for the PFO modeling and 0.50 M for the PSO modelling are relatively low and the fitted q_e values show deviation with the experimental results. Therefore, it can be concluded that adsorption data follow PSO kinetics with $[FA]_0$ of 0.05 M and PFO kinetics with $[FA]_0$ of 0.50 M as shown in Figure 2. The rest of the kinetics modeling is included in Figures S1-S2 (Supporting Information).

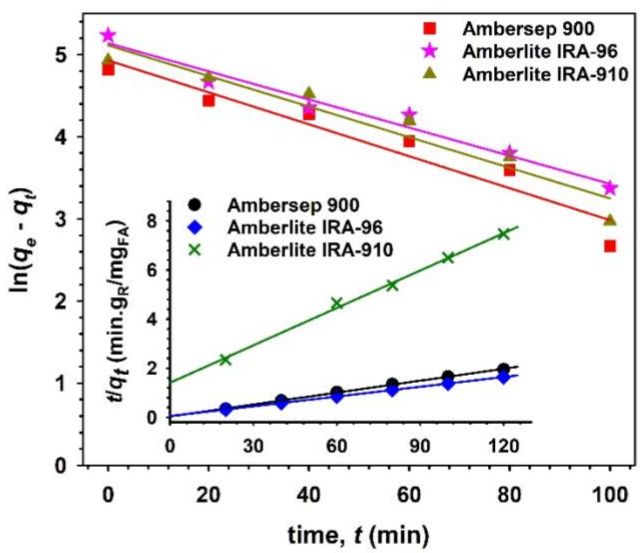

Figure 2. Pseudo first order kinetics modelling for formic acid (FA) adsorption on Ambersep 900 (red square), Amberlite IRA-96 (pink star), and Amberlite IRA-910 (yellow triangle) with $[FA]_0$ of 0.50 M and pseudo second order kinetics modelling (inset) for Ambersep 900 (black circle), Amberlite IRA-96 (blue diamond), and Amberlite IRA-910 (green cross) with $[FA]_0$ of 0.05 M in 10.0 mL of aqueous solution with resin loading of 20 mg/mL. Solid line (linear regressions), $[FA]_0$ (initial concentration of formic acid), q_t (adsorption quantity at time t), and q_e (adsorption capacity at equilibrium).

Table 1. Kinetics modeling for the formic acid (FA) adsorption on Ambersep 900, Amberlite IRA-96, and Amberlite IRA-910 using 0.05 M and 0.50 M initial concentration of FA in 10.0 mL of aqueous solution with resin loading of 20 mg/mL.

Model	Constant	$[FA]_0$ (M)	Ambersep 900	Amberlite IRA-96	Amberlite IRA-910
Elovich	α^{i} (mg_{FA}/g_R)	0.05	8.36×10^{14}	2.45×10^{5}	1.03
		0.50	4.34	10.27	3.93
	β^{ii} (g_R/mg_{FA})	0.05	0.64	0.18	0.20
		0.50	0.02	0.02	0.02
	R^2	0.05	0.71	0.92	0.82
		0.50	0.92	0.91	0.94
PFO	q_e^{iii} (mg_{FA}/g_R)	0.05	17.88	36.64	18.29
		0.50	138.23	170.43	165.99
	k_1^{iv} (1/min)	0.05	0.03	0.04	0.03
		0.50	0.02	0.02	0.02
	R^2	0.05	0.66	0.92	0.95
		0.50	0.92	0.97	0.92
PSO	q_e^{iii} (mg_{FA}/g_R)	0.05	62.11	75.76	19.69
		0.50	250.00	250.00	1666.67
	k_2^{v} (g_R/mg_{FA}/min)	0.05	9.57×10^{-6}	8.90×10^{-6}	3.63×10^{-3}
		0.50	8.64×10^{-6}	3.41×10^{-6}	2.84×10^{-7}
	R^2	0.05	0.999	1.00	1.00
		0.50	0.813	0.92	0.42

[i]Elovich adsorption constant, [ii]Elovich desorption constant, [iii]equilibrium adsorption capacity, [iv]pseudo first order rate constant, [v]pseudo second order rate constant, mg_{FA}/g_R (milligrams of formic acid per gram of resin), $[FA]_0$ (initial formic acid concentration), PFO (pseudo first order), and PSO (pseudo second order), and R^2 (correlation coefficient).

The initial concentration of FA has a large effect on both rate of the reaction and the kinetics order. At low FA initial concentration, the rate depends on both time of contact and concentration of FA with PSO kinetics. This is because of the large number of available surface sites on resin for the adsorption of smaller number FA. As a result, the rate depends on concentration of FA and follows PFO kinetics. The fitted rate constant with $[FA]_0 = 0.05$ M shows that Amberlite IRA-910 has the highest k_2 values compared to the others but at high $[FA]_0 = 0.50$ M, all three resins have almost similar rate constants, k_1 (Table 1).

3.3. Effects of resin dose and formic acid concentration on adsorption. Adsorption experiments were performed with varying resin dose (10–60 mg/mL), and formic acid initial concentrations ($[FA]_0$) of 0.05-2.00 M. The influence of resin doses on FA adsorption capacity for each of the resins is shown in Figure 3, where the adsorption efficiency is presented in Figure S3 (Supporting Information). All three resins show an increase of adsorption capacity with increasing $[FA]_0$ and reaches a maximum at very high $[FA]_0$ representing a *type-I* adsorption isotherm.[13]

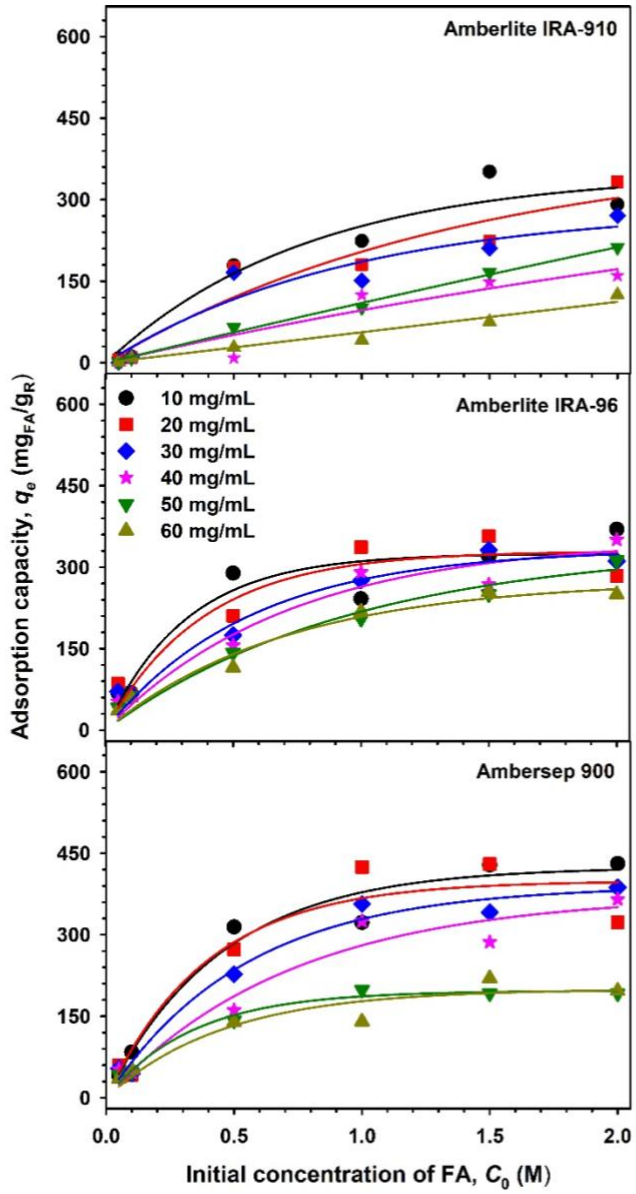

Figure 3. Formic Acid (FA) adsorption capacity of Ambersep 900 (bottom), Amberlite IRA-96 (middle), and Amberlite IRA-910 (top) with resin dose level of 10 mg/mL (black circle), 20 mg/mL (red square), 30 mg/mL (blue diamond), 40 mg/mL (pink star), 50 mg/mL (green triangle down), and 60 mg/mL (yellow triangle down) in 10.0 mL of aqueous solution with varying FA initial concentration in the range of 0.05–2.00 M .

The adsorption capacity of $[FA]_o$ from 0.05 M to 0.50 M is calculated at 40.4 to 430.8 mg_{FA}/g_R for Ambersep 900, 69.2 to 369.9 mg_{FA}/g_R for amberlite IRA-96, and 8.3 to 291.2 mg_{FA}/g_R for

Amberlite IRA-910. With high resin dose level of 60 mg/mL, the adsorption capacity is found as 35.3 to 196.7 mg_{FA}/g_R for Ambersep 900, 35.4 to 250.0 mg_{FA}/g_R for amberlite IRA-96, and 1.7 to 125.3 mg_{FA}/g_R for Amberlite IRA-910.

The adsorption efficiency of $[FA]_o$ from 0.05 M to 0.50 M is calculated as 19.0 to 4.5 % for Ambersep 900, 32.6 to 4.6 % for Amberlite IRA-96, and 0.1 to 6.7 % for Amberlite IRA-910. With the high resin dose level of 60 mg/mL, the adsorption efficiency is calculated as 99.9 to 12.3% for Ambersep 900, 99.9 to 16.3% for amberlite IRA-96, and 4.8 to 7.8 % for Amberlite IRA-910. All other intermediate dose levels of the resins (20-50 mg/mL) had similar trends for equilibrium adsorption capacity and adsorption efficiency, where the increase of $[FA]_0$ increases the adsorption capacity while decreasing the adsorption efficiency. It is also noted here that at a fixed $[FA]_0$, the adsorption capacity drops with increases in the resin dose level along with rises in adsorption efficiency. This could be explained that for the same number of FA molecules the resins surface sites increase with increasing dose level, but the site utilization does not increase commensurately. As a result, adsorption capacity goes down and corresponding adsorption efficiency goes up. This effect is clearly observed for all three resins with varying resin doses and FA concentration levels.

To understand the effects of $[FA]_0$ on adsorption capacity and adsorption efficiency with resin doses, the data is replotted with different *x*-axis in Figure S4 and Figure S5 (Supporting information). At highest $[FA]_0$ of 2.00 M, the equilibrium adsorption capacity and adsorption efficiency decreases and increases, respectively, with increase in resin dose in faster rate at the lower level of resin dose, at high level of resin doses this drop is almost constant meaning saturation of surface by FA. This trend is very similar to an intermediate level of $[FA]_o$ with 1.50, 1.00 and 0.50 M. However, at very low levels of $[FA]_0$ with 0.10 and 0.05 M, the resin dose has minimum effects on adsorption capacity and could be because at this level of $[FA]_0$ the lowest dose of resin has been already saturated by the available FA molecules, hence even if resin dose level rises, it has no impact on adsorption capacity.

3.4. Adsorption mechanism: adsorption capacity and resins basicity. With all levels of resin doses and FA concentration, Ambersep 900 shows the highest adsorption capacity. The adsorption capacity trends from FA aqueous solution are as follows: Ambersep 900 hydroxide form > Amberlite IRA-96 ≈ Amberlite IRA-910 chloride form. However, the extent of adsorption capacity varies with initial FA concentration and resin dose levels. This may be due to the difference in the exchangeable ionic group and functional group attached to the resin of same matrix (styrene/divinylbenzene polymer) affecting the basicity of the resin and hence the relative interaction of resin and formic acid/formate. The adsorption capacity and selectivity of anion exchange resins are typically correlated with physical or chemical interaction, usually electrostatic, covalent, and non-covalent interaction of the desired species.[13, 39, 56, 57] The strongly basic anion exchange resins (SBAs) are generally quaternary ammonium derivatives, where their functional groups are completely dissociated irrespective to their ionic form and pH of the solution.[13, 57] The SBAs are sub-divided into two groups, type I with slightly higher basicity (Ambersep 900 hydroxide form) and affinity than their type II counterparts (Amberlite IRA-910 chloride form).[47, 57] On the other hand, primary, secondary, or tertiary amine or their mixtures and/or derivatives belong to the weakly basic anion exchange resins.[39, 56, 58] Amberlite IRA-96 free base form from this category has been chosen for current study due to the presence of a lone pair of electrons on the nitrogen atoms of its functional groups which can act as a Lewis base. Based on the solution pH, this resin therefore can exist in solution as a free base and its ionized form. Based on the structures and speciation mentioned in Table S1, the basicity order for the three resins can be ordered as follows: Ambersep 900 hydroxide form > Amberlite IRA-910 chloride form >> Amberlite IRA-96. The fraction of dissociated and undissociated formic acid (a single acid dissociation constant, K_a of 1.77×10^{-4}) will be determined by the pH of the solution and pK_a of formic acid (3.75) as shown by Henderson−Hasselbalch equation (equation 15).[13, 59]

$$p^{H} = p^{K_a} + \log\frac{[HCOO^-]}{[HCOOH]} \quad \ldots\ldots 15$$

This equation indicates that below pH = 3.75, almost all the FA molecules in the solution are undissociated, whereas above that value, they are fully dissociated. The FA remains mostly in undissociated form in the experimental concentration ranges for the aqueous solution of FA of 0.05-2.00 M, with pH values ranging from 1.75 to 3.15. In real CO_2RR for cathode using 0.5 M $KHCO_3$ solution saturated with humid CO_2 with a wide range of initial formic acid concentration (0.005 M to 2.5 M) the solution pH falls from 8.1 to 2.1 as shown in Figure S6. Produced formic acid can stay both in dissociated and undissociated state in catholyte mixture of real CO_2RR cathode chamber and binding with AER will be affected. The interaction of undissociated and dissociated formic acid with three resins under different modes is shown in Scheme 1 and explained as follows.

Amberlite IRA-96 free base form with its nitrogen lone pair of electrons can form hydrogen bond with hydroxyl group of FA. Therefore, separation of formic acid will happen due to this type of interaction with this resin. Unlike the Amberlite IRA-96 free base form, both Amberlite IRA-910 and Ambersep 900 in aqueous solutions are fully dissociated in their ionic forms with chloride and hydroxide anion where the liberated hydroxide and chloride can act as base taking up the proton from formic acid. Therefore, under these conditions the Ambersep 900 will have more available dissociated formic acid compared to Amberlite IRA-910 as chloride is less basic than hydroxide. As a result, the formic acid separation is driven by ion-ion interaction of the resin on Ambersep 900. Amberlite IRA-910 can also form hydrogen bond with the undissociated formic acid by its ethanolic hydroxyl groups with the formic acid hydroxyl groups in addition to ion-ion interactions. The highest adsorption capacity for Ambersep 900 hydroxide form can be explained by its highly basic character and ion-ion separation. Although the Amberlite IRA-910 chloride form is more basic than Amberlite IRA-96 free base form, the almost equal adsorption capacity of Amberlite IRA-910 chloride form may be due to dual interaction of ion-ion separation and hydrogen bonded covalent interactions.

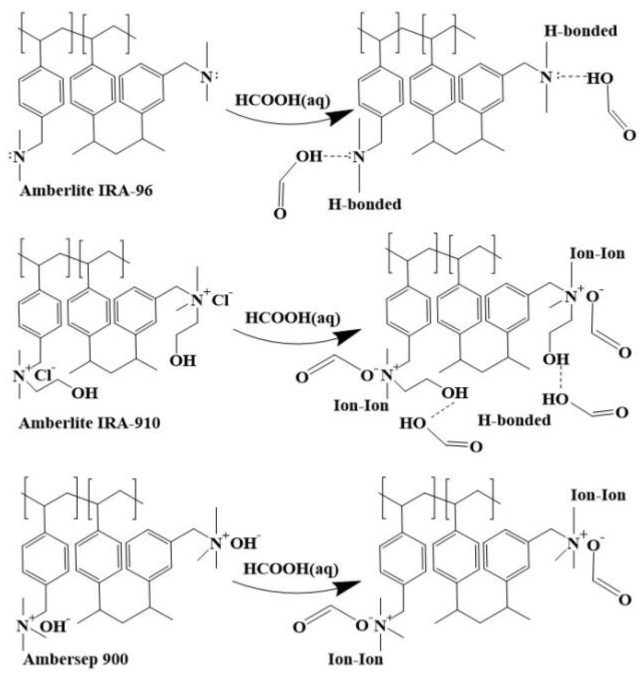

Scheme 1. Adsorption mode of formic acid from aqueous solution on Ambersep 900 (bottom), Amberlite IRA-910 (middle) and Amberlite IRA-96 (top) with Ion-Ion and H-bonded separation. (Structures based on information provided by the manufacturers.)

3.5. Adsorption isotherms modeling. Langmuir, Freundlich, and Temkin isotherm models were employed to understand the FA adsorption on the three anion exchange resins. The Langmuir model assumes the monolayer adsorption of FA on the homogenous resin surface. According to this model, only one molecule can adsorb on a specific site with a single adsorption event on that specific available site.[60] The adsorption energy remains uniform at each adsorption site without any interaction. The mathematical expression of this model along with linear form is shown in equation 9 and 10.[60]

$$\text{Langmuir; } q_e = q_{max}\frac{K_L C_e}{1+K_L C_e} \ldots\ldots 9$$

$$\text{Linear form of Langmuir; } \frac{C_e}{q_e} = \frac{C_e}{q_{max}} + \frac{1}{K_L q_{max}} \ldots\ldots 10$$

Where q_e is the adsorption capacity at equilibrium, q_{max} is the maximum adsorption capacity, K_L is the Langmuir equilibrium constant related to affinity of adsorbent site and energy of adsorption, and C_e is the equilibrium FA concentration in the bulk solution. The dimensionless separation factor (R_L) defined by equation 11 tells if the isotherm is favorable ($0 < R_L < 1$), unfavorable ($R_L > 1$), linear ($R_L = 1$), or irreversible ($R_L = 0$).[61]

$$\text{Separation factor; } R_L = \frac{1}{1+K_L C_0} \ldots\ldots 11$$

The Freundlich model assumes multilayer and non-uniform adsorption of solute molecules on the heterogenous resin surfaces. The isotherm model and linear plot are given by the equation 12 and 13.[62]

$$\text{Freundlich; } q_e = K_F[C_e]^{\frac{1}{n}} \ldots\ldots 12$$

$$\text{Linear form of Freundlich; } \log q_e = \log K_F + \frac{1}{n}\log[C_e] \ldots\ldots 13$$

Where, K_F is the Freundlich adsorption capacity and n is the Freundlich adsorption intensity, and its reverse parameter 1/n indicates a measure of sorption intensity or surface heterogeneity ($0 < 1/n < 1$), and as the value of $1/n$ got closer to 0, the sorption became more heterogeneous and cooperative sorption ($1/n > 1$).[54, 62] The Temkin adsorption isotherm model (equation 14) describes the adsorption on equilibrium data, where system has heterogenous surfaces and non-uniform adsorption heat distributions. This model assumes the heat of sorption of solute molecules decrease linearly with surface coverage caused by the solute-resin interactions.[63]

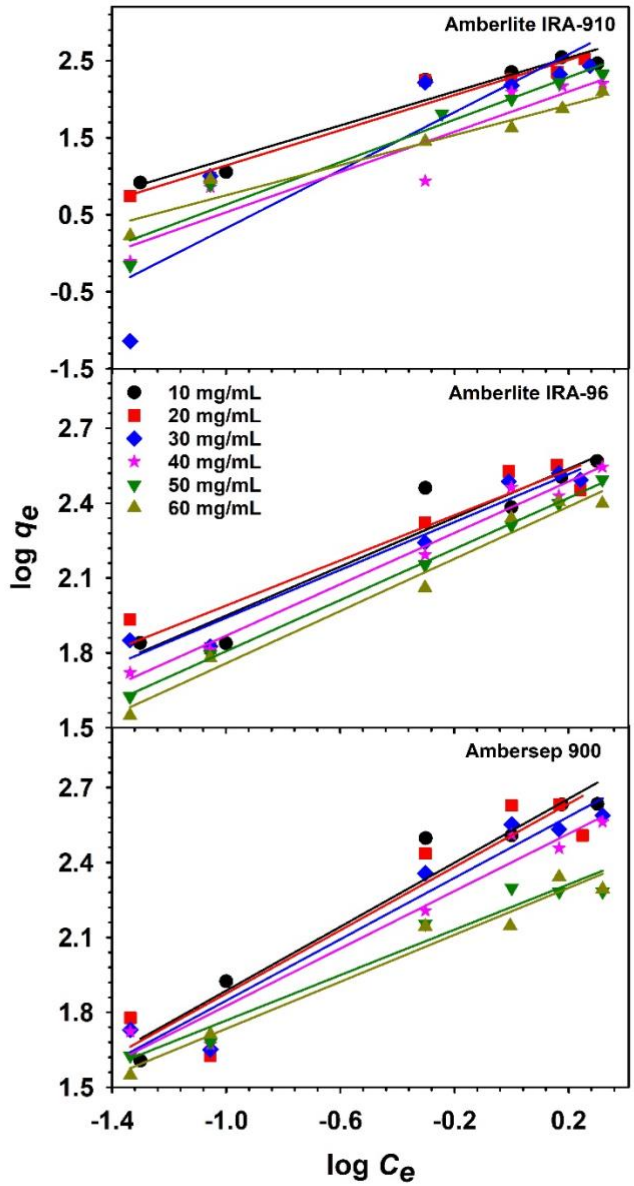

Figure 4. Freundlich isotherm model for the adsorption of formic acid (FA) on Ambersep 900 (bottom), Amberlite IRA-96 (middle), and Amberlite IRA-910 (top) with resin dose level of 10 mg/mL (black circle), 20 mg/mL (red square), 30 mg/mL (blue diamond), 40 mg/mL (pink star), 50 mg/mL (green triangle down), and 60 mg/mL (yellow triangle up) in 10.0 mL of aqueous solution for varying FA initial concentration in the range of 0.05–2.00 M. q_e; equilibrium adsorption capacity, and C_e; equilibrium FA concentration.

$$\text{Temkin; } q_e = \frac{RT}{B}\ln K_T + \frac{RT}{B}\ln C_e \ldots\ldots\ldots\ldots 14$$

where, B and K_T are the Temkin equilibrium-binding constant and Temkin constant related to the adsorption heat, respectively. Using the experimental data for equilibrium adsorption capacity and concentration, all three models' linear equations are used. Figure 4 shows the Freundlich model for the three resins, with the Langmuir and Temkin models in Figure S7-S8 (Supporting Information).

The isotherms modeling constants are calculated and listed in Table S3-S5. The separation factor, R_L ($0 < R_L < 1$) and Freundlich reverse adsorption intensity, $1/n$ ($0 < 1/n < 1$) describes the favorability and reversibility of the adsorption process for the Langmuir and Freundlich models, respectively.[64] The values for R_L and $1/n$ obtained from the linear regression analysis from the experimental concentration range show that FA adsorptions with Langmuir and Freundlich model are favorable for both Ambersep 900 and Amberlite IRA-910. The linear regression correlation coefficient (R^2) of Langmuir and Freundlich model can better describe the adsorption process within a certain range for both Ambersep 900 and Amberlite IRA-96, whereas the Freundlich model is more predictable for Amberlite IRA-910. The fitted equilibrium adsorption capacity (q_e) from Freundlich model is a good match with the experimental data. Therefore, it can conclude that based on the values obtained from linear regression for R_L, $1/n$, R^2, and q_e the Freundlich model is more suitable to predict the adsorption process, suggesting that FA adsorption onto the surface of the resin is heterogenous. The equilibrium adsorption capacity from this model (Table S3-S5) predicts the order of three resins' adsorption capacity as Ambersep 900 (336.7 mg_{FA}/g_R) > Amberlite IRA-96 (275.2 mg_{FA}/g_R) > Amberlite IRA-910 (209.2 mg_{FA}/g_R).

3.6. Effects of potassium bicarbonate on adsorption capacity and adsorption efficiency. Potassium bicarbonate has been widely used as catholyte for CO_2 conversion with a concentration range of 0.1-1.0 M in H-type and flow cell.[65-69] Here, 0.5 M $KHCO_3$ aqueous solution with varying FA level is used with resin doses of 10 and 60 mg/mL to model FA separation from a realistic electrocatalytic CO_2 reduction experimental setup. The adsorption capacity profiles are shown in Figure 5. In the previous sections, the adsorption of FA from aqueous solution on Ambersep 900, Amberlite IRA-96, and Amberlite IRA-910 have been studied with three adsorption models. Ambersep 900, Amberlite IRA-96, and Amberlite IRA-910 follow Freundlich model with corresponding maximum equilibrium adsorption capacity of 336.7 for Ambersep 900, 275.2 for Amberlite IRA-96, and 209.2 mg_{FA}/g_R for Amberlite IRA-910 without $KHCO_3$ in 10 mg/mL resin. But the corresponding equilibrium FA adsorption capacity drops to 40.0 for Ambersep 900, 110.8 for Amberlite IRA-96, and 99.9 mg_{FA}/g_R for Amberlite IRA-910 in presence of potassium bicarbonate (Table 2). The maximum equilibrium adsorption capacity of each resin with neutral water and potassium bicarbonate aqueous solution are summarized in Figure 6. A similar trend in terms of a drop in FA adsorption capacity at a 60 mg/mL resin loading is observed in the presence of potassium bicarbonate. The potassium bicarbonate also has a negative impact on the adsorption capacity of resins (q_e plotted in Figure S8, Supporting Information).

To better understand the effects of $KHCO_3$ on FA adsorption, the data is replotted as a mole fraction of potassium bicarbonate in the inset of Figure 5. This shows that increasing the mole fraction of potassium bicarbonate drops the adsorption capacity suggesting the competitive adsorption of possibly bicarbonate and formate ion on resin surface. To further confirm the effects of mole fraction of $KHCO_3$, experiment with 0.20 M initial concentrations of $KHCO_3$ with 60 mg/mL loading are performed and similar trends to that of 0.50 M are observed in Figure S8 (Supporting Information).

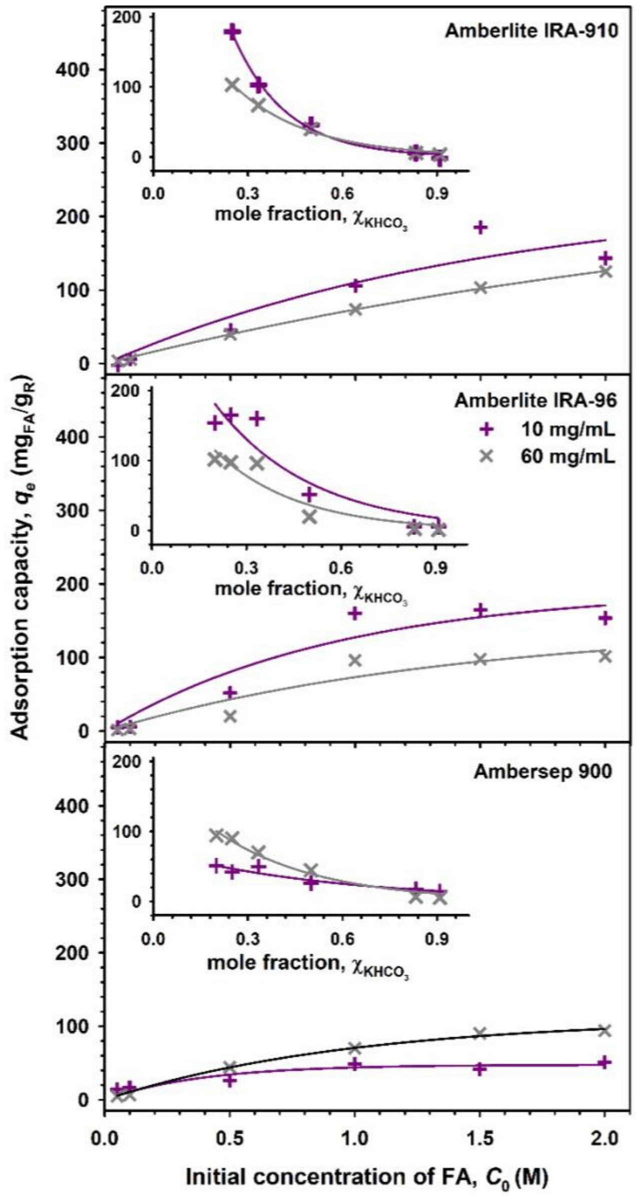

Figure 5. Effects of potassium bicarbonate ($KHCO_3$) on Formic Acid (FA) adsorption capacity of Ambersep 900 (bottom), Amberlite IRA-96 (middle), and Amberlite IRA-910 in 10.0 mL of 0.50 M $KHCO_3$ aqueous solution with varying FA initial concentrations of 0.05–2.00 M and resin dose of 10 mg/mL (pink plus) and 60 mg/mL (grey cross). The adsorption capacity with the mole fraction of potassium bicarbonate (χ_{KHCO_3}) is on the inset for Ambersep 900 (bottom), Amberlite IRA-96 (middle), and Amberlite IRA-910 (top).

The adsorption efficiency of the resins with varying $KHCO_3$ initial concentration and resin loading are depicted in Figure S10-S11 (Supporting Information). For $[KHCO_3]_0$ = 0.20 M with very low $[FA]_0$ of 0.05 M, the adsorption efficiency is higher until the formic acid concentration increases to 0.50 M. After that the adsorption efficiency remains almost constant with further increases in $[FA]_0$. In the case of $[KHCO_3]_0$ = 0.50 M, the adsorption efficiency remains almost constant at any level of $[FA]_0$ from 0.05 M to 0.50 M. This indicates that formic acid and potassium bicarbonate have some level of competitive adsorptions for these three resins. When the formic acid concentration is too low, $[FA]_0$ = 0.05 compared to bicarbonate $[KHCO_3]_0$ = 0.20 M, almost all the formic acid can be separated by resins. In case of $[KHCO_3]_0$ = 0.50 M, bicarbonate is much higher than formic acid, $[FA]_0$ = 0.05 M at the beginning, with more bicarbonate getting adsorbed on the resins and less formic acid separation.

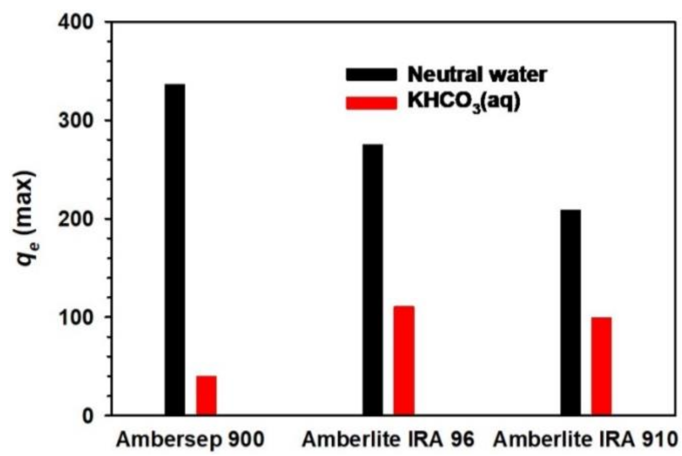

Figure 6. Maximum FA adsorption capacity of resins at equilibrium from neutral water (red bar) and potassium bicarbonate aqueous solution (black bar) with Freundlich modelling,

3.7. Effects of potassium bicarbonate on adsorption isotherm. The adsorption data in the presence of $KHCO_3$ are fitted to Langmuir (Figure S12, Supporting Information), Freundlich (Figure 7), and Temkin (Figure S13, Supporting Information) models with their corresponding linear equations as described earlier. The isotherms modeling constants are calculated from the slopes and intercepts of the linear regression analysis and listed in Table 2. The linear regression correlation coefficient (R^2) for all three resins can again best be described by a Freundlich model, where the R^2 is too low for both Langmuir and Temkin models. The higher values of $1/n$ obtained from the linear regression analysis with the Freundlich model for Ambersep 900 indicates more competitive adsorption on that surface compared to the other resins.[62] This also supports the lower adsorption capacity of Ambersep 900 in presence of the potassium bicarbonate. The equilibrium adsorption capacity (q_e) obtained from the Freundlich isotherm plot is a better matched with the experimental data. Considering those assessments, the adsorption isotherm in the presence of the potassium bicarbonate is more suitable to predict the FA adsorption process using the Freundlich model suggesting FA adsorption onto the surface of resin is heterogenous and competitive. Similar behaviors in the adsorption isotherms modeling and their parameters are observed with 0.20 M potassium bicarbonate as depicted in Figure S14-S16 and listed in Table S6 (Supporting Information).

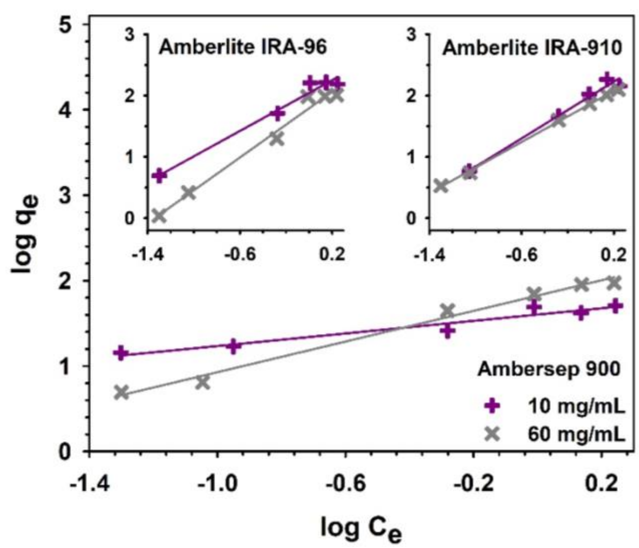

Figure 7. Freundlich isotherm model for formic acid (FA) adsorption on Ambersep 900, Amberlite IRA-96 (left inset), Amberlite IRA-910 (right inset) in 10.0 mL of 0.50 M potassium bicarbonate ($KHCO_3$) aqueous solution with varying FA concentrations of 0.05–2.00 M and resin doses of 10

mg/mL (pink solid plus) and 60 mg/mL (grey solid cross). Lines are for corresponding linear regressions.

Table 2. Isotherm modelling data for the formic acid (FA) adsorption on resins from 10.0 mL of 0.50 M $KHCO_3$ aqueous solution with varying FA initial concentrations of 0.05–2.00 M and resin dose level of 10 and 60 mg/mL.

Model	resin dose (mg/mL)	q_{max}[vi] (mg_{FA}/g_R)	R_L[vii]	K_L[viii] (mg_{FA}/mL)	R^2
Langmuir	10[a]	55.9	0.14 – 0.86	13.6	0.927
	60[a]	384.6	0.73 – 0.99	221.3	0.300
	10[b]	-285.5×10^3	1.00 - 1.00	-123.5×10^3	0.001
	60[b]	-61.7	1.02 – 3.95	-107.1	0.692
	10[c]	-416.7	1.00 - 1.32	-257.0	0.291
	60[c]	-1428.6	1.00 – 1.08	-960.1	0.213
	resin dose (mg/mL)	K_F[ix] (mg_{FA}/g_R)	$1/n$[x]		R^2
Freundlich	10[a]	40.1	0.37		0.935
	60[a]	66.9	0.90		0.989
	10[b]	110.8	1.03		0.978
	60[b]	62.2	1.34		0.982
	10[c]	99.0	1.16		0.980
	60[c]	74.0	1.04		0.999
	resin dose (mg/mL)		K_T[xi] (mL/mg_{FA})	B[xii] (mJ/mg_{FA})	R^2
Temkin	10[a]		61.9	5.37	0.875
	60[a]		16.8	2.09	0.960
	10[b]		12.8	1.16	0.845
	60[b]		14.1	1.69	0.904

10[c]	17.5	1.18	0.837
60[c]	13.0	1.77	0.841

[vi]maximum adsorption capacity, [vii]separation factor, [viii]Langmuir equilibrium constant, [ix]Freundlich adsorption capacity, [x]Freundlich adsorption intensity, [xi]Temkin equilibrium-binding constant and [xii]Temkin constant related to the heat of adsorption, [a]Ambersep 900, [b]Amberlite IRA-96, [c]Amberlite IRA-910, R^2 (correlation coefficient), mg_{FA}/g_R (milligrams of formic acid per gram of resin, mg_{FA}/mL (milligrams of formic acid per mL of solution), mJ/mg_{FA} (millijoules per milligram of formic acid), mL/mg_{FA} (mL of volume of solution per milligrams of formic acid).

4. CONCLUSIONS

The formic acid adsorption kinetics and adsorption capacity of strongly basic Ambersep 900, less strongly basic Amberlite IRA-910, and weakly basic Amberlite IRA-96 with varying formic acid initial concentration were studied and fit well with second order kinetics at low $[FA]_0$ and first order kinetics at high $[FA]_0$ for all three anion exchange resins. All three of these resins follow the Freundlich model for heterogeneous adsorption for formic acid from an aqueous (water) solution and show competitive adsorption in presence of a potassium bicarbonate electrolyte. The maximum adsorption capacity with Freundlich model of 336.7, 275.2, and 209.2 mg_{FA}/g_R is found from the neutral water, but decreased in the presence of $KHCO_3$ to 40.0, 110.8, and 99.9 mg_{FA}/g_R for Ambersep 900, Amberlite IRA-96, and Amberlite IRA-910, respectively. Although the strongly basic Ambersep 900 has a maximum FA adsorption capacity compared to weakly basic Amberlite IRA-96 and less strongly basic Amberlite IRA-910 from the aqueous solution, the presence of potassium bicarbonate has a more severe negative effect on the resin adsorption. The weakly basic Amberlite IRA-96 and Amberlite IRA-910 show viable adsorption capacities in the range of 99 - 110 mg_{FA}/g_R even with some competitive adsorption from the potassium bicarbonate. Assessment of the ion exchange regeneration process, including energy consumption and chemical usage, will be needed to inform corresponding life-cycle and techno-economic assessments to further compare the benefits of producing formate/formic acid with electrocatalytic CO_2R versus more conventional methods.

SUPPORTING INFORMATION

Characteristic features and operating conditions of resins (Table S1); Isotherm modeling data for the formic acid (FA) adsorption on resins with varying resin doses and FA initial concentrations (Table S2-S4); Isotherm modeling data for the formic acid (FA) adsorption on resins with varying concentrations of $KHCO_3$ aqueous solution with varying FA concentrations (Table S5); Isotherms data with 0.20 M $KHCO_3$ experiment (Table S6); Elovich, pseudo first order, and pseudo second order kinetics at different initial concentration of formic acid (Figures S1−S2); Formic acid adsorption efficiency of anion exchange resins with varying initial formic acid concentration and resin loading from aqueous solution (Figure S3-S4); Formic acid adsorption capacity of anion exchange resins with varying initial formic acid concentration and resin loading from aqueous solution (Figure S5); Variation of saturated pH of the model catholyte solution mixture of CO2RR (Figure S6); Langmuir and Temkin isotherm modeling with varying initial formic acid concentration and resin loading from aqueous solution (Figure S7-S8); Effects of potassium bicarbonate on formic acid adsorption efficiency and adsorption capacity (Figure S9-S11); Langmuir, Freundlich, and Temkin isotherm modeling in presence potassium bicarbonate (Figure S12-S16). This information is available free of charge via the internet at http://pubs.acs.org/

AUTHOR INFORMATION

Corresponding Author

Jesse Thompson

*Email: jesse.thompson@uky.edu

Phone: 859-257-0355

ORCID: 0000-0001-7193-4685

Notes

The authors declare no competing financial interest.

ACKNOWLEDGMENT

This material is based upon work supported by the Department of Energy under Award Number DE-FE0031920.

ABBREVIATIONS

CO_2RR, CO_2 Reduction Reaction; FA, Formic Acid; LCA, Life-cycle Analysis; CCU, Carbon Capture and Utilization; CCS, Carbon Capture and Storage; CF, Carbon Footprint; AER, Anion Exchange Resin; FB, Free Base; PFO, Pseudo First Order; PSO, Pseudo Second Order; $[FA]_0$, Initial Formic Acid Concentration; $[KHCO_3]_0$, Initial Potassium Bicarbonate Concentration.

REFERENCES

1. Kennedy, J. F.; Shimizu, J. *Chemical Fixation of Carbon Dioxide Methods for Recycling CO_2 into Useful Products*. Elsevier: CRC Press Inc., Boca Raton, Florida, 1995; 26, 67-127.
2. Aresta, M. *Carbon Dioxide as Chemical Feedstock*. John Wiley & Sons: Weinheim, Germany, 2010; XV, 1-13.
3. Aresta, M.; Dibenedetto, A. Utilisation of CO_2 as a Chemical Feedstock: Opportunities and Challenges. *Dalton Trans.* **2007,** 28, 2975-2992.
4. Whipple, D. T.; Kenis, P. J. A. Prospects of CO_2 Utilization via Direct Heterogeneous Electrochemical Reduction. *J. Phys. Chem. Lett.* **2010,** 1(24), 3451-3458.

5. Quadrelli, E. A.; Centi, G.; Duplan, J. L.; Perathoner, S. Carbon dioxide recycling: emerging large-scale technologies with industrial potential. *ChemSusChem.* **2011,** 4(9), 1194-1215.
6. Fan, L.; Xia, C.; Zhu, P.; Lu, Y.; Wang, H. Electrochemical CO_2 Reduction to High-concentration Pure Formic Acid Solutions in an All-Solid-State Reactor. *Nat. Commun.* **2020,** 11(1), 1-9.
7. Ma, W.; Xie, S.; Zhang, X.-G.; Sun, F.; Kang, J.; Jiang, Z.; Zhang, Q.; Wu, D.-Y.; Wang, Y. Promoting Electrocatalytic CO_2 Reduction to Formate via Sulfur-Boosting Water Activation on Indium Surfaces. *Nat. Commun.* **2019,** 10(1), 1-10.
8. Scialdone, O.; Galia, A.; Nero, G. L.; Proietto, F.; Sabatino, S.; Schiavo, B. Electrochemical Reduction of Carbon Dioxide to Formic Acid at a Tin Cathode in Divided and Undivided Cells: Effect of Carbon Dioxide Pressure and Other Operating Parameters. *Electrochim. Acta.* **2016,** *199*, 332-341.
9. Agarwal, A. S.; Zhai, Y.; Hill, D.; Sridhar, N. The Electrochemical Reduction of Carbon Dioxide to Formate/Formic Acid: Engineering and Economic Feasibility. *ChemSusChem.* **2011,** 4(9), 1301-1310.
10. Lu, X.; Leung, D. Y. C.; Wang, H.; Leung, M. K. H.; Xuan, J. Electrochemical Reduction of Carbon Dioxide to Formic Acid. *ChemElectroChem.* **2014,** *1*(5), 836-849.
11. Li, L.; Yang, J.; Li, L.; Huang, Y.; Zhao, J. Electrolytic Reduction of CO_2 in $KHCO_3$ and Alkanolamine Solutions with Layered Double Hydroxides Intercalated with Gold or Copper. *Electrochim. Acta.* **2022,** *402*, 139523.
12. Salazar-Villalpando; D., M. Effect of Electrolyte on the Electrochemical Reduction of CO_2. *ECS Transac.* **2011,** *33* (27), 77.
13. Zeidan, H.; Marti, M. E. Separation of Formic Acid from Aqueous Solutions onto Anion Exchange Resins: Equilibrium, Kinetic, and Thermodynamic Data. *J. Chem. Eng. Data.* **2019,** *64* (6), 2718-2727.
14. Bhandari, V. M.; Juvekar, V. A.; Patwardhan, S. R. Sorption Studies on Ion Exchange Resins. 2. Sorption of Weak Acids on Weak Base Resins. *Ind. Eng. Chem. Res.* **1992,** *31* (4), 1073-1080.
15. Cai, W.; Zhu, S.; Piao, X. Extraction Equilibria of Formic and Acetic Acids from Aqueous Solution by Phosphate-Containing Extractants. *J. Chem. Eng. Data.* **2001,** *46* (6), 1472-1475.
16. Grasemann, M.; Laurenczy, G. Formic Acid as a Hydrogen Source–Recent Developments and Future Trends. *Energy Environ. Sci.* **2012,** *5* (8), 8171-8181.
17. Rahbari, A.; Ramdin, M.; Van Den Broeke, L. J. P.; Vlugt, T. J. H. Combined Steam Reforming of Methane and Formic Acid to Produce Syngas with an Adjustable H_2: CO Ratio. *Ind. Eng. Chem. Res.* **2018,** *57* (31), 10663-10674.
18. Madsen, M. R.; Rønne, M. H.; Heuschen, M.; Golo, D.; Ahlquist, M. S. G.; Skrydstrup, T.; Pedersen, S. U.; Daasbjerg, K. Promoting Selective Generation of Formic Acid from CO_2 Using Mn (bpy)$(CO)_3$Br as Electrocatalyst and Triethylamine/Isopropanol as Additives. *J. Am. Chem. Soc.* **2021,** *143* (48), 20491-20500.
19. Huan, T. N.; Andreiadis, E. S.; Heidkamp, J.; Simon, P.; Derat, E.; Cobo, S.; Royal, G.; Bergmann, A.; Strasser, P.; Dau, H. From Molecular Copper Complexes to Composite Electrocatalytic Materials for Selective Reduction of CO_2 to Formic Acid. *J. Mater. Chem. A* **2015,** *3* (7), 3901-3907.

20. Roy, S.; Sharma, B.; Pécaut, J.; Simon, P.; Fontecave, M.; Tran, P. D.; Derat, E.; Artero, V. Molecular Cobalt Complexes with Pendant Amines for Selective Electrocatalytic Reduction of Carbon Dioxide to Formic Acid. *J. Am. Chem. Soc.* **2017,** *139* (10), 3685-3696.
21. Van Daele, K.; De Mot, B.; Pupo, M.; Daems, N.; Pant, D.; Kortlever, R.; Breugelmans, T. Sn-based Electrocatalyst Stability: A Crucial Piece to the Puzzle for the Electrochemical CO_2 Reduction Toward Formic Aacid. *ACS Energ. Lett.* **2021,** *6* (12), 4317-4327.
22. Zheng, T.; Liu, C.; Guo, C.; Zhang, M.; Li, X.; Jiang, Q.; Xue, W.; Li, H.; Li, A.; Pao, C.-W. Copper-catalysed Exclusive CO_2 to Pure Formic Acid Conversion via Single-Atom Alloying. *Nat. Nanotechnol* **2021,** *16* (12), 1386-1393.
23. Duarah, P.; Haldar, D.; Yadav, V. S. K.; Purkait, M. K. Progress in the Electrochemical Reduction of CO_2 to Formic Acid: A Review on Current Trends and Future Prospects. *J. Environ. Chem. Eng.* **2021,** *9* (6), 106394.
24. Ding, P.; Zhao, H.; Li, T.; Luo, Y.; Fan, G.; Chen, G.; Gao, S.; Shi, X.; Lu, S.; Sun, X. Metal-based Electrocatalytic Conversion of CO_2 to Formic Acid/Formate. *J. Mater. Chem. A* **2020,** *8* (42), 21947-21960.
25. Yang, H.; Kaczur, J. J.; Sajjad, S. D.; Masel, R. I. Performance and Long-Term Stability of CO_2 Conversion to Formic acid using a Three-Compartment Electrolyzer Design. *J. CO_2 Util.* **2020,** *42*, 101349.
26. Yang, H.; Kaczur, J. J.; Sajjad, S. D.; Masel, R. I. Electrochemical Conversion of CO_2 to Formic Acid Utilizing Sustainion™ Membranes. *J. CO_2 Util.* **2017,** *20*, 208-217.
27. Kaczur, J. J.; McGlaughlin, L. J.; Lakkaraju, P. S. Investigating Pervaporation as a Process Method for Concentrating Formic Acid Produced from Carbon Dioxide. *C.* **2020,** *6* (2), 42.
28. Birdja, Y. Y.; Shen, J.; Koper, M. T. M. Influence of the Metal Center of Metalloprotoporphyrins on the Electrocatalytic CO_2 Reduction to Formic Acid. *Catal. Today.* **2017,** *288*, 37-47.
29. Kaneco, S.; Hiei, N.-H.; Xing, Y.; Katsumata, H.; Ohnishi, H.; Suzuki, T.; Ohta, K. High-efficiency Electrochemical CO_2-to-Methane Reduction Method using Aqueous $KHCO_3$ Media at less than 273 K. *J. Solid State Electrochem.* **2003,** *7* (3), 152-156.
30. Ávila-Bolívar, B.; Montiel, V.; Solla-Gullón, J. Electrochemical Reduction of CO_2 to Formate on Nanoparticulated Bi−Sn−Sb Electrodes. *ChemElectroChem.* **2022,** *9* (9), e202200272.
31. Zhao, C.; Li, Y.; He, Z.; Jiang, Y.; Li, L.; Jiang, F.; Zhou, H.; Zhu, J.; Meng, W.; Wang, L. $KHCO_3$ Activated Carbon Microsphere as Excellent Electrocatalyst for VO^{2+}/VO_2^+ Redox Couple for Vanadium Redox Flow Battery. *J. Energ. Chem.* **2019,** *29*, 103-110.
32. Guo, W.; Zhang, Y.; Su, J.; Song, Y.; Huang, L.; Cheng, L.; Cao, X.; Dou, Y.; Ma, Y.; Ma, C. Transient Solid-State Laser Activation of Indium for High-Performance Reduction of CO_2 to Formate. *Small* **2022**, 2201311.
33. Li, T.; Lees, E. W.; Zhang, Z.; Berlinguette, C. P. Conversion of Bicarbonate to Formate in an Electrochemical Flow Reactor. *ACS Energy Lett.* **2020,** *5* (8), 2624-2630.
34. Kannan, N.; Xavier, A. New Composite Mixed Adsorbents for the Removal of Acetic Acid by Adsorption from Aqueous Solutions-a Comparative Study. *Toxicol. Environ. Chem.* **2001,** *79* (1-2), 95-107.
35. Marti, M. E. Recovery of Formic Acid by Reactive Extraction using an Environmentally Friendly Solvent. *Selcuk Univ. J. Eng., Sci. Technol.* **2017,** *5* (1), 26-37.

36. Belova, V. V.; Zakhodyaeva, Y. A.; Voshkin, A. A. Extraction of Carboxylic Acids with Neutral Extractants. *Theor. Found. Chem. Eng.* **2017,** *51* (5), 786-794.
37. Yang, S.-T.; Huang, H.; Tay, A.; Qin, W.; De Guzman, L.; San Nicolas, E. C. Extractive Fermentation for the Production of Carboxylic Acids. In *Bioprocessing for Value-Added Products from Renewable Resources*, Elsevier: Dublin, Ohio, 2007; 421-446.
38. Pursell, M. R.; Mendes-Tatsis, M. A.; Stuckey, D. C. Coextraction During Reactive Extraction of Phenylalanine using Aliquat 336: Modeling Extraction Equilibrium. *Biotechnol.* **2003,** *82* (5), 533-542.
39. Uslu, H. Adsorption Equilibria of Formic Acid by Weakly Basic Adsorbent Amberlite IRA-67: Equilibrium, Kinetics, Thermodynamic. *Chem. Eng. J.* **2009,** *155* (1-2), 320-325.
40. Rasrendra, C. B.; Girisuta, B.; Van de Bovenkamp, H. H.; Winkelman, J. G. M.; Leijenhorst, E. J.; Venderbosch, R. H.; Windt, M.; Meier, D.; Heeres, H. J. Recovery of Acetic Acid From an Aqueous Pyrolysis Oil Phase by Reactive Extraction using Tri-*n*-octylamine. *Chem. Eng. J.* **2011,** *176*, 244-252.
41. Hietala, J.; Vuori, A.; Johnsson, P.; Pollari, I.; Reutemann, W.; Kieczka, H. *Formic Acid*. Ullmann's Encyclopedia of Industrial Chemistry: Berlin, Germany, 2016; Vol. 1, p 1-22.
42. Wang, W.; Himeda, Y.; Muckerman, J. T.; Manbeck, G. F.; Fujita, E. CO_2 Hydrogenation to Formate and Methanol as an Alternative to Photo-and Electrochemical CO_2 Reduction. *Chem. Rev.* **2015,** *115* (23), 12936-12973.
43. Maru, M. S.; Ram, S.; Shukla, R. S.; Noor-ul, H. K. Ruthenium-Hydrotalcite (Ru-HT) as an Effective Heterogeneous Catalyst for the Selective Hydrogenation of CO_2 to Formic Acid. *Mole. Catal.* **2018,** *446*, 23-30.
44. Ramdin, M.; Morrison, A. R. T.; De Groen, M.; Van Haperen, R.; De Kler, R.; Irtem, E.; Laitinen, A. T.; Van Den Broeke, L. J. P.; Breugelmans, T.; Trusler, J. P. M. High-pressure Electrochemical Reduction of CO_2 to Formic Acid/Formate: Effect of pH on the Downstream Separation Process and Economics. *Ind. Eng. Chem. Res.* **2019,** *58* (51), 22718-22740.
45. Aldaco, R.; Butnar, I.; Margallo, M.; Laso, J.; Rumayor, M.; Dominguez-Ramos, A.; Irabien, A.; Dodds, P. E. Bringing Value to the Chemical Industry from Capture, Storage and Use of CO_2: A Dynamic LCA of Formic Acid Production. *Sci. Total Environ.* **2019,** *663*, 738-753.
46. Rumayor, M.; Dominguez-Ramos, A.; Irabien, A. Formic Acid Manufacture: Carbon Dioxide Utilization Alternatives. *Appl. Sci.* **2018,** *8* (6), 914.
47. Lin, X.; Xiong, L.; Huang, C.; Yang, X.; Guo, H.; Chen, X.; Chen, X. Sorption Behavior and Mechanism Investigation of Formic Acid Removal by Sorption Using an Anion-Exchange Rresin. *Desalin. Water Treat.* **2016,** *57* (1), 366-381.
48. De Gisi, S.; Lofrano, G.; Grassi, M.; Notarnicola, M. Characteristics and Adsorption Capacities of Low-cost Sorbents for Wastewater Treatment: A Review. *Sustain. Mater. Technol.* **2016,** *9*, 10-40.
49. Barbaro, P.; Liguori, F. Ion Exchange Resins: Catalyst Recovery and Recycle. *Chem. Rev.* **2009,** *109* (2), 515-529.
50. Van Deventer, J. Selected Ion Exchange Applications in the Hydrometallurgical Industry. *Solvent Extr. Ion Exch.* **2011,** *29* (5-6), 695-718.
51. Liu, B.-J.; Hu, Z.-J.; Ren, Q.-L. Single-Component and Competitive Adsorption of Levulinic/Formic Acids on Basic Polymeric Adsorbents. *Colloids Surf. A.* **2009,** *339* (1-3), 185-191.

52. Treigerman, Z.; Sasson, Y. Separation of Formate Ion from a Catalytic Mixture After a Hydrogenation Process of Bicarbonate Ion and Generation of Formic Acid-The Last Stage of the Formic Acid Cycle. *Am. J. Anal. Chem.* **2019,** *10* (8), 296-315.
53. Smith, R. M.; Martell, A. E. *Critical Stability Constants: Second Supplement*. Springer: New York, 1989; 6.
54. Tan, I. A. W.; Ahmad, A. L.; Hameed, B. H. Adsorption Isotherms, Kinetics, Thermodynamics and Desorption Studies of 2, 4, 6-Trichlorophenol on Oil Palm Empty Fruit Bunch-Based Activated Carbon. *J. Hazard. Mater.* **2009,** *164* (2-3), 473-482.
55. Ho, Y. S.; McKay, G. Kinetic Models for the Sorption of Dye from Aqueous Solution by Wood. *Process Saf. Environ. Prot.* **1998,** *76* (2), 183-191.
56. Wołowicz, A.; Hubicki, Z. Investigation of Macroporous Weakly Basic Anion Exchangers Applicability in Palladium (II) Removal from Acidic Solutions–Batch and Column Studies. *Chem. Eng. J.* **2011,** *174* (2-3), 510-521.
57. Wołowicz, A.; Hubicki, Z. Comparison of Strongly Basic Anion Exchange Resins Applicability for the Removal of Palladium (II) Ions from Acidic Solutions. *Chem. Eng. J.* **2011,** *171* (1), 206-215.
58. Bhandari, V. M.; Yonemoto, T.; Juvekar, V. A. Investigating the Differences in Acid Separation Behaviour on Weak Base Ion Exchange Resins. *Chem. Eng. Sci.* **2000,** *55* (24), 6197-6208.
59. Po, H. N.; Senozan, N. M. The Henderson-Hasselbalch Equation: Its History and Limitations. *J. Chem. Edu.* **2001,** *78* (11), 1499.
60. Langmuir, I. The Constitution and Fundamental Properties of Solids and Liquids. Part I. Solids. *J. Am. Chem. Soc.* **1916,** *38* (11), 2221-2295.
61. Weber, T. W.; Chakravorti, R. K. Pore and Solid Diffusion Models for Fixed-Bed Adsorbers. *AIChE J.* **1974,** *20* (2), 228-238.
62. Freundlich, H. Über Die Adsorption in Lösungen. *Zeitschrift Für Physikalische Chemie* **1907,** *57* (1), 385-470.
63. Temkin, M. I. Kinetics of Ammonia Synthesis on Promoted Iron Catalysts. *Acta Phys. Chim. USSR* **1940,** *12*, 327-356.
64. Hu, L.; Zheng, J.; Li, Q.; Tao, S.; Zheng, X.; Zhang, X.; Liu, Y.; Lin, X. Adsorption of 5-Hydroxymethylfurfural, Levulinic Acid, Formic Acid, and Glucose using Polymeric Resins Modified with Different Functional Groups. *ACS Omega.* **2021,** *6* (26), 16955-16968.
65. Rasouli, A. S.; Wang, X.; Wicks, J.; Lee, G.; Peng, T.; Li, F.; McCallum, C.; Dinh, C.-T.; Ip, A. H.; Sinton, D.; Sargent, E. H. CO_2 Electroreduction to Methane at Production Rates Exceeding 100 mA/cm^2. *ACS Sustainable Chem. Eng.* **2020,** *8* (39), 14668-14673.
66. Li, H.; Oloman, C. Development of a Continuous Reactor for the Electro-Reduction of Carbon Dioxide to Formate–Part 1: Process Variables. *J. Appl. Electrochem.* **2006,** *36* (10), 1105-1115.
67. Sassone, D.; Zeng, J.; Fontana, M.; Farkhondehfal, M. A.; Pirri, C. F.; Bocchini, S. Highly Dispersed Few-nanometer Chlorine-doped SnO_2 Catalyst Embedded in a Polyaniline Matrix for Stable $HCOO^-$ Production in a Flow Cell. *ACS Appl. Mater. Interfaces* **2022,** *14* (37), 42144-42152.
68. Meng, Y.; Zhang, X.; Hung, W.-H.; He, J.; Tsai, Y.-S.; Kuang, Y.; Kenney, M. J.; Shyue, J.-J.; Liu, Y.; Stone, K. H. Highly Active Oxygen Evolution Integrated with Efficient CO_2 to CO Electroreduction. *PNAS* **2019,** *116* (48), 23915-23922.

69. Zhai, Y.; Chiachiarelli, L.; Sridhar, N. Effect of Gaseous Impurities on the Electrochemical Reduction of CO_2 on Copper Electrodes. *ECS Transac.* **2009,** *19* (14), 1.

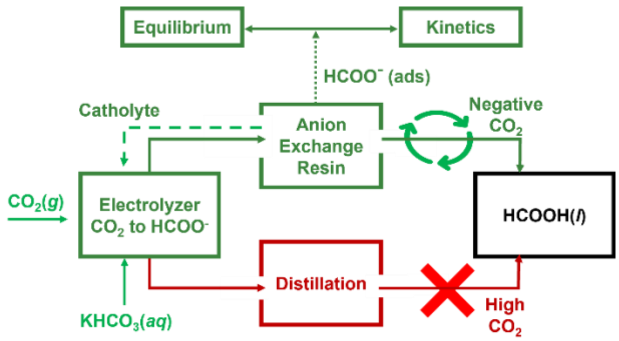

" For Table of Contents Only"